Rev. Roum. Sci. Techn.– Électrotechn. et Énerg.
Vol. **70**, *2*, pp. 175–180, Bucarest, 2025

ANALYSIS OF WIND TURBINE POWER OUTPUT VIA MODELING, SIMULATION, AND VALIDATION

CIPRIAN POPA[1], NICOLAE-SILVIU POPA[1*], FLORENȚIU DELIU[2], OVIDIU CRISTEA[2], IANCU CIOCIOI[2], MIHAI-OCTAVIAN POPESCU[1]

Keywords: Electrical power generation; Experimental validation; Mathematical modeling; Renewable energy; Wind turbine.

This paper presents a comprehensive study on the mathematical modeling, simulation, and experimental validation of the electrical power output of a wind turbine system. The research begins with developing mathematical models to determine the useful electrical power generated by the wind turbine under varying operational conditions. These models are then simulated using MATLAB/Simulink to predict the system's performance. A physical prototype of the wind turbine system is constructed to collect experimental data under real-world conditions. Finally, the experimental results are compared with the simulated data to validate the accuracy of the mathematical models. The maximum relative error observed between the simulated and experimental data is 1.71 %, highlighting the reliability of the proposed models. The research demonstrates the effectiveness of the mathematical approach for predicting wind turbine performance and offers valuable insights into the design and optimization of small-scale wind energy systems.

1. INTRODUCTION

The world is facing significant challenges, including the depletion of fossil fuels, rising carbon emissions, and climate change [1]. In response, there is an increasing shift towards cleaner and more sustainable energy alternatives to mitigate environmental impacts. Renewable energy sources, like wind energy, are being adopted to reduce dependency on fossil fuels, lower carbon footprints, and improve air quality. Wind energy has rapidly established itself as one of the most widely adopted and fastest-growing renewable resources worldwide [2–6].

Wind energy production begins by capturing the kinetic energy of moving air, which drives turbine blades to generate mechanical power. This mechanical energy is converted into electrical power via a generator for various applications [7–10]. As a sustainable and eco-friendly energy source, wind power plays a pivotal role in the global shift toward renewable energy. It reduces fossil fuel dependence, lowers greenhouse gas emissions, and improves air quality, aligning with environmental goals and promoting the long-term sustainability of energy systems [11–13].

Wind turbines play a central role in wind energy systems and are generally categorized into two main types: Horizontal-Axis Wind Turbines (HAWT) and Vertical-Axis Wind Turbines (VAWT) [8, 10, 14]. HAWTs are generally more favored because they operate based on the principle of aerodynamic lift, which allows them to achieve higher efficiency in energy extraction compared to VAWTs, which rely on drag forces. Although HAWTs are more complex in terms of construction and typically incur higher costs, their superior performance in capturing wind energy makes them the preferred choice for large-scale energy production. This combination of aerodynamic principles and performance efficiency contributes significantly to their popularity in the renewable energy sector [15,16].

This study explores the mathematical modeling of electrical energy production from a HAWT. The objective is to construct accurate theoretical models that estimate the turbine's effective power output, perform simulations using MATLAB (Simulink), and analyze the results. Subsequently, an experimental setup will be developed to gather real-world data, which will be used to validate the accuracy of the simulated outcomes. The findings are intended to verify the reliability of the proposed models and support advancements in wind turbine efficiency within renewable energy applications.

2. MATHEMATICAL MODELS

HAWT generate electricity by capturing the kinetic energy of the wind, which is then converted into mechanical energy as the blades rotate [17]. As the wind passes over the blades, it causes them to spin, capturing the wind's energy. This mechanical rotational energy is then transmitted to a generator, where it undergoes a final transformation into electrical power that can be utilized in various applications. This sequential energy conversion process makes wind turbines an effective and sustainable source of renewable electricity [18–20].

To calculate the kinetic energy (E_c) of an air mass moving at a velocity v_1 (m/s), the following equation is applied [18]:

$$E_c = \frac{m * v_1^2}{2}, \tag{1}$$

where m represents the mass flow rate of the moving air (kg/s), influenced by air density ρ and the cross-sectional area S (m^2) of the airflow considered. ,hese factors combine to determine the total available energy that the wind turbine can harness.

With the appropriate data regarding air density, exposed surface area, and wind speed, the available power of the airflow can be calculated, expressed in watts [18].

$$P_{available} = \frac{\rho S v_1^3}{2}. \tag{2}$$

The wind turbine's energy output is influenced by the power coefficient C_p and the wind energy available, as expressed through the following:

$$P = C_p * \frac{\rho S v_1^3}{2}. \tag{3}$$

The coefficient C_p, also known as the efficiency coefficient, represents how efficiently a wind turbine harnesses energy from the wind. Based on theoretical limits, no wind turbine can extract more than 59 % of the wind's kinetic energy. This restriction, known as the Betz limit, is a core concept in wind turbine theory, which states that only a portion of the total wind energy can be converted into mechanical energy [18].

[1] Faculty of Electrical Engineering, National University of Science and Technology Politehnica Bucharest, Romania.
E-mails: ciprian.popa2904@stud.electro.upb.ro, nicolae_silviu.popa@stud.electro.upb.ro (Correspondence address), mo.popescu@upb.ro
[2] Marine Engineering Faculty, "Mircea cel Bătrân" Naval Academy, Romania.
E-mails: florentiu.deliu@anmb.ro, ovidiu.cristea@anmb.ro, iancu.ciocioi@anmb.ro

DOI: 10.59277/RRST-EE.2025.2.4

It is characterized as the proportion of power captured by the turbine relative to the total power present in the wind flow. This can be mathematically represented as [18]:

$$C_p(\lambda,\beta) = c_1\left(\frac{c_2}{\lambda_i} - c_3\beta - c_4\right)e^{\frac{-c_5}{\lambda_i}} + c_6\lambda, \quad (4)$$

where λ_i is defined as:

$$\frac{1}{\lambda_i} = \frac{1}{\lambda + 0{,}08\beta} - \frac{0{,}035}{\beta^3 + 1} \quad \mathbf{(5)}$$

The values for the parameters c_1 to c_6 are as follows: c_1 = 0.5176, c_2 = 116, c_3 = 0.4, c_4 = 0, c_5 = 21, and c_6 = 0.0068. The maximum power coefficient C_p is achieved when β = 0, representing the rotor blades' pitch angle.

The relationship between the tip speed ratio and the power coefficient typically characterizes the aerodynamic performance of a turbine blade. The tip speed ratio, denoted as λ, is described as the ratio of the tangential velocity of the blade tip to the wind speed entering the flow tube [18].

$$\lambda = \frac{v_t}{v_1} = \frac{\omega_r * R}{v_1}, \quad (6)$$

$$\omega_r = \frac{2\Pi n}{60}, \quad (7)$$

where ω_r stands for the angular velocity of the rotor [rad/s], R is the rotor radius [m], and n refers to the rotational speed of the rotor [rot/min].

The mechanical power obtained is determined using the relation [18]:

$$P_m = \eta_m * C_p * \frac{\rho S v_1^3}{2} \quad (8)$$

To calculate the generated electrical power, the formula used is [18]:

$$P_e = \eta_e * \eta_m * C_p * \frac{\rho S v_1^3}{2} \quad (9)$$

Finally, the useful electrical power can be obtained as follows [18]:

$$P_u = \eta_{aux} * \eta_e * \eta_m * C_p * \frac{\rho S v_1^3}{2} \quad (10)$$

where η_m, represents the overall efficiency of the mechanical transmission system; η_e, is the efficiency of the electric generator; η_{aux}, refers to the efficiency of auxiliary circuits [18].

To calculate the turbine's effective electrical output power, we applied eqs. (4)-(7) in conjunction with equation (10), which led to the following expression:

$$P_u = \eta_{aux}\eta_e\eta_m\left\{c_1\left[c_2\left(\frac{1}{\frac{2\Pi n\cdot R}{60 v_1}+0{,}08\beta} - \frac{0{,}035}{\beta^3+1}\right) - c_3\beta - c_4\right]e^{-c_5\left(\frac{1}{\frac{2\Pi n\cdot R}{60 v_1}+0{,}08\beta} - \frac{0{,}035}{\beta^3+1}\right)} + c_6\frac{2\Pi n\cdot R}{60 v_1}\right\}\cdot\frac{\rho S v_1^3}{2}. \quad (11)$$

3. SIMULATION OF WIND CONVERSION

A block diagram for a HAWT will be developed in MATLAB (Simulink) to facilitate the analysis and simulation of its performance song as well as the various phenomena that arise during operation. This step involves formulating the mathematical relationships that describe the interaction between the turbine, wind, generator, and other system components. To determine the performance coefficient, C_p, the block diagram has been designed using the formulas presented in sections 4 and 5:

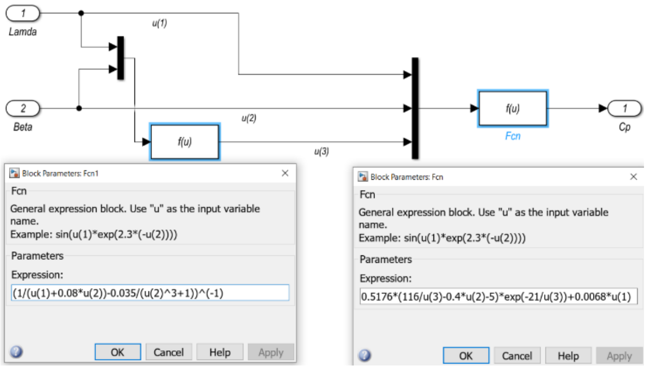

Fig. 1 – The block diagram of the turbine's performance coefficient, C_p.

To better illustrate the mathematical algorithm and how the power coefficient, C_p, along with the available wind energy, determines the mechanical power generated by a wind turbine, we will proceed by modeling the block diagram based on eq. (8). This highlights the key relationships between essential parameters and the turbine's operational performance.

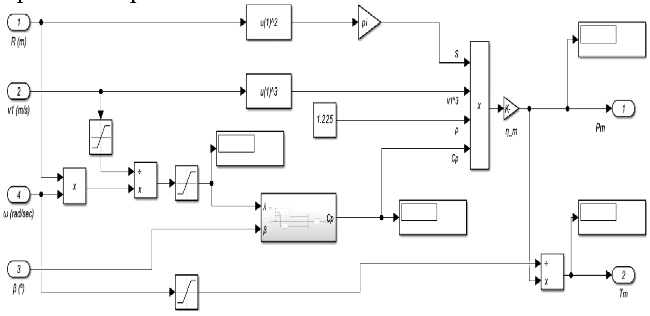

Fig. 2 – Block diagram of the mechanical power, P_m.

Accurate simulation results required determining a value for η_m, which proved challenging due to incomplete technical specifications of the wind turbine. Mechanical losses were approximated using typical values for small turbines: friction losses from high-quality bearings (1-3 % of total power) and negligible internal aerodynamic friction (1-2 %). Consequently, the mechanical efficiency of the transmission system was estimated at 97 %, with losses attributed to bearings (2 %) and internal aerodynamic friction (1 %).

FoT generator's efficiency was 95 % for the experimental setup, and the wind controller's efficiency, representing auxiliary circuits, was evaluated at 97 %. These parameters were integrated into the Simulink block diagram to calculate the effective electrical power generated by the turbine, as defined by eq. (11).

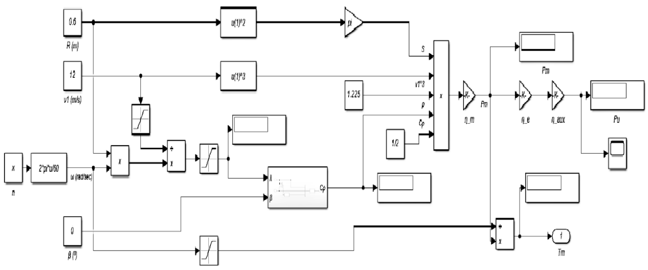

Fig. 3 – Block diagram of useful electric power, P_u.

Figure 4 incorporates eq. (7) into the block diagram to calculate the rotor's angular velocity based on its rotational speed. This step is essential since a tachometer will gather experimental data at various wind speeds. The rotor's rotational speed will serve as an input parameter for the simulation.

4. SIMULATED RESULTS

To maximize simulation accuracy, input values were derived from experimental measurements. Wind speed was recorded using an anemometer, and rotor rotational speed was measured with a tachometer. This approach directly compared simulated and experimental results, ensuring a strong correlation. The simulations offered detailed insights into system performance across various operating conditions, providing valuable data for validating the proposed model.

Table 1

A part of the simulated results.

Current number	Date measured		Simulated results
	v1 [m/s]	n [rot/min]	Pu [W]
1.	4	137	6.98
2.	4.8	164	12.00
3.	5	172	13.76
4.	5.8	202	22.10
5.	7.2	229	35.10
6.	9.5	253	62.27
7	7.6	235	39.31

These results provide a foundational basis for the subsequent simulated phase and are crucial for further optimizing the design.

Upon examining the diagram of the simulated values, it is evident that the electrical power output from the wind turbine increases in direct proportion to wind speed. This relationship indicates that as **wind speed increases, the energy captured by the rotor also increases, leading to higher electrical power generation.**

The mathematical model was precisely calibrated by utilizing experimental data (wind speed) as input parameters in the simulation to ensure accurate alignment between theory and experiment. The simulations produced detailed insights into the system's performance, including the electrical power generated by the wind turbine.

These results will later be compared with data gathered from practical tests conducted under real-world conditions to validate the model in an actual environment.

5. EXPERIMENTAL DESIGN OF THE WIND SYSTEM

We developed a wind system optimized for varying testing conditions using the resources and equipment provided by the "Renewable Energy Sources and Electrical Equipment Maintenance" laboratory at the "Mircea cel Bătrân" Naval Academy. The design process involved the careful selection of components and their integration into a system capable of efficiently generating and managing the energy produced by a horizontal-axis wind turbine (HAWT). The completed system, operating independently, consists of key elements like the controller, storage batteries, and the inverter.

For this section, we selected an HAWT with a power rating of 200 W, as a larger turbine was not required for the experimental results. The wind system controller is critical in safeguarding the storage batteries by preventing overcharging and deep discharging. Additionally, it acts as a rectifier, transforming the alternating current produced by the wind turbine into direct current, which is required for battery charging and supplying power to connected equipment.

Fig. 4 – HAWT with a power rating of 200 W.

We have adapted the wind system by incorporating battery accumulators, which ensure extended operational life and allow for efficient management of stored energy. These accumulators provide a continuous energy supply even during low wind conditions.

To achieve a 24 V system, we created a configuration that combines series and parallel connections between the AGM batteries. Initially, two batteries were connected in series to achieve a total voltage of 24 V, with each battery contributing 12 V. This series connection ensures that the total voltage is the sum of the individual battery voltages.

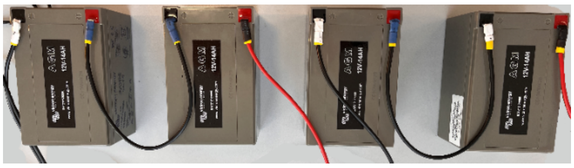

Fig. 5 – The storage system with a capacity of 28 Ah at 24 V.

To increase the storage capacity, we added two groups of series-connected batteries, which were then connected in parallel. Each group provides 24 V in this configuration, and the parallel connection increased the storage capacity from 14 Ah to 28 Ah, resulting in a final storage system of 28 Ah at 24 V.

The battery storage system was not designed based on a precise calculation of the necessary energy capacity, considering all the consumers requiring power. Instead, it was created to provide short-term autonomy due to the limited resources available.

The final key component was the inverter, which was selected and configured to convert the stored energy in the batteries from direct current (DC) to alternating current (AC), including the AC generated by the wind turbine, ensuring the system's power needs were met. The inverter was tested to confirm its ability to handle the required power demands, minimizing energy losses efficiently.

Fig. 6 – The 24V inverter with an apparent power of 500 VA.

Within the wind turbine system, a variable load setup was implemented to simulate different loading conditions and force the system to operate at its maximum capacity. This system comprises five incandescent light bulbs connected in parallel, each controlled by a dedicated switch. The bulbs used include three 60W and two 100W bulbs. This strategic configuration was selected to maximize energy extraction from the wind system and controller. Without this variable load setup, the wind system and controller would be unable to meet the system's energy production capacity, thereby failing to meet consumers' needs, which would result in an underestimate of the system's energy production capacity.

Fig. 7 – Physical realization of variable loads system.

To gather and analyze relevant experimental data regarding the performance of the wind system, it was necessary to integrate a data acquisition board into the system's structure. We used the CerboS-GX board from Victron Energy, an advanced device that facilitates real-time monitoring and data retrieval at one-minute intervals. This integration was crucial for obtaining precise and up-to-date information about the wind system's operation, enabling a detailed assessment of its operational parameters and efficiency under various usage conditions.

Fig. 8 – Data acquisition board, CerboS-GX

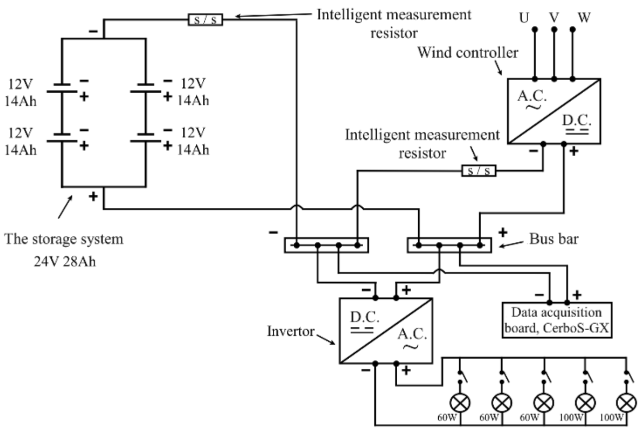

Fig. 9 – Electrical schematic of the autonomous wind system.

Regarding the battery systems and the wind controller, an intelligent measurement resistor was necessary on the negative terminal of each component. These resistors were connected to the data acquisition board via the VE cable, enabling precise monitoring of current and voltage and thus ensuring a detailed and comprehensive collection of experimental data from the entire system.

After analyzing and detailing all the essential components for constructing an autonomous wind system, we moved on to the practical phase of design and implementation. In this stage, we developed the electrical schematic of the entire system, which included the connections and interactions between the wind generator, the charge controller, the battery bank, the inverter, and the variable load consumer system.

Based on this electrical schematic, we implemented the physical system, which facilitated the collection of significant experimental data, including voltage, current, generated power, and system efficiency, under various operating conditions. This data was used to evaluate experimental performance and validate the simulated mathematical model.

6. EXPERIMENTAL RESULTS

After the physical construction was completed, the wind system was installed on the roof of the Faculty of Marine Engineering at the “Mircea cel Bătrân” Naval Academy. The initial purpose of this installation was to adjust the functional parameters of the controller, the smart measurement resistors, and the inverter, and to calibrate the data acquisition board to ensure accurate monitoring of essential variables. The electrical connections were also optimized to reduce losses and improve energy efficiency. Subsequently, experimental data were collected.

Data were monitored and transmitted to the acquisition board via the smart measurement resistor connected to the negative terminal of the output from the wind controller. The recorded parameters included the charging current, voltage, battery charging power, and the useful electrical power produced by the HAWT.

F. Fig. 10 – Measuring wind speed with a WT816A anemometer

In this study, electrical parameters were acquired in real time at one-minute intervals via the SmartShunt measurement resistor and transmitted to the data acquisition board, as illustrated in Fig. 11. Meanwhile, wind speed was manually recorded every 10 minutes using a WT816A anemometer positioned near the wind turbine. These readings were crucial for evaluating the impact of wind conditions on system behavior. Simultaneously, the rotor speed was measured with a handheld tachometer, allowing the turbine's angular velocity to be calculated. All manually acquired data were subsequently interpolated to match the resolution of the electrical measurements, ensuring accurate comparison and validation of the simulated results.

The experimental data for the wind system were collected between August 2 and September 13, 2024, covering a range of wind conditions, including days with low wind intensity. However, the simulation models were based on measurements taken on August 28, 2024, during a day characterized by moderate wind. For the final analysis, only the most relevant data were selected, specifically those corresponding to stronger wind gusts when the data acquisition board recorded significant electrical parameters.

Table 2

A part of the experimental results.

Current number	Date measured v1 [m/s]	n [rot/min]	Experimental results Pu [W]
1.	4	137	7.09
2.	4.8	164	12.01
3.	5	172	14.00
4.	5.8	202	22.44
5.	7.2	229	35.27
6.	9.5	253	62.59
7	7.6	235	39.19

These experimental data are crucial for confirming and validating the simulated system model. The accuracy of the theoretical model will be evaluated by comparing the results from the practical tests with the simulated data, highlighting any differences or inconsistencies.

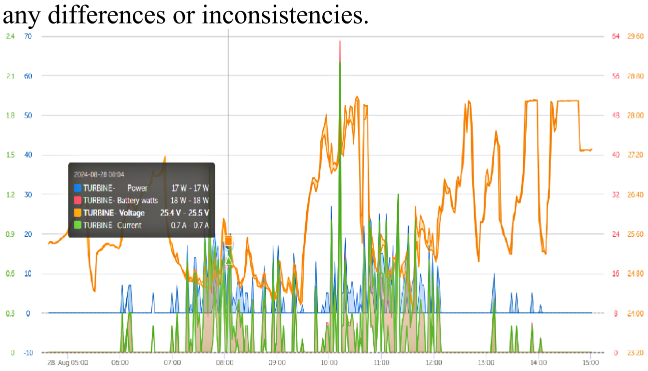

Fig. 11 – All HAWT's parameters recorded by the smart shunt.

The acquisition board gathered experimental data sent by the smart measurement resistor, which tracked essential parameters from the wind controller's output, such as the useful electrical power produced by the HAWT, along with current, voltage, and battery charging power. These parameters will be utilized to verify the wind system's performance.

Monitoring the wind turbine's electrical output and the power used for battery charging revealed discrepancies between actual values and those recorded by the smart resistor connected to the wind controller's output. This device provides rounded measurements without decimals, introducing approximation errors. For example, at 17.43 W, the turbine's output is recorded as 17 W, and at 17.85 W, it shows 17 W for the turbine, but 18 W for charging power. These differences arise from the resistor's rounding method: turbine values are rounded down, while charging values are rounded to the nearest integer, leading to less accurate estimates under certain conditions.

Data on battery charging voltage and current were also used to address this issue. These parameters allowed for a more precise correlation between experimental data and those obtained from simulations regarding the turbine's generated power.

7. VALIDATION OF EXPERIMENTAL AND SIMULATED DATA

The previous sections described all the steps and input data leading to the simulated and actual results. To validate the simulated results against the experimental ones, we calculated the relative error, which expresses the difference as a percentage of the experimental value, helping to gauge the significance of the error in relation to the measured electrical power. The formula for relative error is:

$$E_R = \frac{\left|Value_{experimental} - Value_{simulated}\right|}{\left|Value_{experimental}\right|} 100\ [\%]. \quad (12)$$

Using the error calculation formula and both the experimental and simulated data, a table was developed to emphasize the notable discrepancies between the corresponding values (Table 3).

Table 3

The process of comparing experimental data with simulated results for validation.

Current number	Simulated Pu [W]	Experimental Pu [W]	Error ER [%]
1.	6.98	7.09	1.55
2.	12.00	12.01	0.08
3.	13.76	14.00	1.71
4.	22.1	22.44	1.51
5.	35.1	35.27	0.48
6.	62.27	62.59	0.51
7	39.31	39.19	0.30

The input values, such as air density, the radius of the turbine blades, and the blade pitch angle, were not included in the table as these values remained constant throughout all simulations and did not require further adjustments.

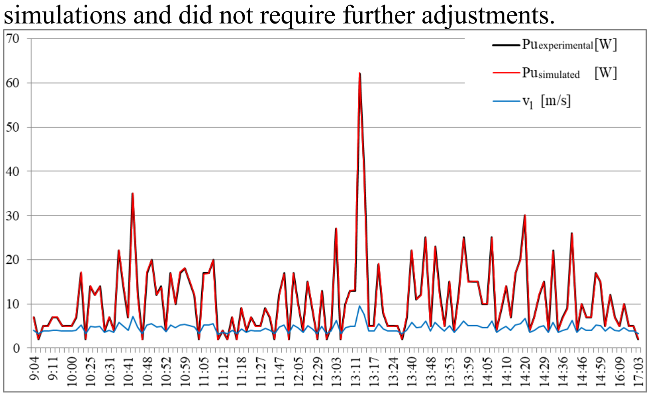

Fig. 12 – Time variation of the real and simulated values of the useful electric power.

By analyzing the relative error values over time, we observed that it fluctuates within a defined range, reaching a minimum value of 0.08 and peaking at 1.71. This range highlights the consistency of the system's accuracy across different operational conditions, with minimal error variations that reflect the precision of the experimental validation in most scenarios. We could compare the simulated values with those obtained from actual experiments by applying the relative error calculation method, highlighting any minor discrepancies. This approach allowed for a detailed evaluation of the model's accuracy, enabling valuable insights into potential improvements that may be necessary. With the relative error kept below 1.72 %, we can conclude that the developed mathematical model accurately reflects the behavior of the wind system, proving to be a reliable tool for future analyses and predictions.

8. **CONCLUSIONS**

The study validates the accuracy and reliability of the developed mathematical models for a small-scale wind turbine, with a maximum relative error of 1.71 % between simulated and experimental results.

A significant original contribution lies in designing and implementing a functional experimental prototype, which confirmed the accuracy of the developed mathematical model through practical testing. Furthermore, an autonomous wind system was engineered to perform reliably under fluctuating and demanding environmental conditions. The formulated mathematical approach also demonstrates flexibility, allowing for future integration of additional renewable energy sources.

CREDIT AUTHORSHIP CONTRIBUTION STATEMENT

Ciprian Popa: Responsible for the design and installation of the system, collecting experimental and simulated data, and writing articles.
Nicolae-Silviu Popa: Responsible for the design and installation of the system and managing correspondence with the editorial board.
Florentiu Deliu: responsible for the experimental design and system dimensioning.
Ovidiu Cristea: Development/configuration of the data acquisition system.
Iancu Ciocioi: Conducted the literature review and introduction section.
Mihai-Octavian Popescu: Analysis and verification of data consistency, manuscript review, and editing.

Received on 11 January 2025

REFERENCES

1. Y. Dris, M.C. Benhabib, S.M. Meliani, V. Dumbrava, *Performance analysis of a hybrid farm (Photovoltaic system wind turbine) connected to the grid using nine–switches converter*, UPB Sci. Bull. Ser. C Electr. Eng. Comput. Sci., **83**, *3*, pp. 207–224 (2021).
2. A. Boulayoune, A. Oubelaid, A. Chibah, *Comparative study of inner and outer rotor flux reversal permanent magnet machine for direct drive wind turbine*, Rev. Roum. des Sci. Tech. Ser. Electrotech. Energ., **69**, *2*, pp. 123–128 (2024).
3. Y. El–Okda, M.S. Emeara, N. Abdelkarim, K. Adref, H. Al Hajjar, *Performance of a small horizontal axis wind turbine with blade pitching*, 2020 Adv. Sci. Eng. Technol. Int. Conf. ASET 2020 (2020).
4. M. Sivaramakrishnaiah et al., *Numerical and experimental investigations on a bladeless turbine: Tesla's cohesion–type innovation*, Int. J. Renew. Energy Dev., **13**, *1*, pp. 110–121 (2024).
5. M.S. Davis, A. Jafarian, F. Ferdowsi, M.R. Madani, *Wind energy harvesting capability of a novel cascaded dual–rotor horizontal–axis wind turbine*, Int. Conf. Electr. Comput. Commun. Mechatronics Eng. ICECCME 2021 (2021).
6. M. Debbache, F. Meziane, A. Bekhti, M. Tata, *Design and sizing of wind blades based on generator parameters for small wind turbines for low wind regions*, Proc. – 2023 2nd Int. Conf. Electron. Energy Meas. IC2EM 2023 (2023).
7. R. Elumalai, *Maximum power quality tracking of artificial neural network controller–based double fed induction generator for wind energy conversion system*, Rev. Roum. des Sci. Tech. Ser. Electrotech. Energ., **69**, *2*, pp. 189–194 (2024).
8. W.M. Amirul Bin Mohd Adnan, A. Bt Abdul Aziz, L.B. Raya, *Feasibility study of wind power generation system using small scale wind turbines*, 2022 IEEE 10th Conf. Syst. Process Control. ICSPC 2022 – Proc., pp. 166–169 (2022).
9. G. Shahgholian, S.M.A. Zanjani, *A study of voltage sag in distribution system and evaluation of the effect of wind farm equipped with doubly–fed induction generator*, Rev. Roum. des Sci. Tech. Ser. Electrotech. Energ., **68**, *3*, pp. 271–276 (2023).
10. M. Sateesh Kumar, Y.V. Pavan Kumar, D. John Pradeep, C.P. Reddy, *Analysis on the effectiveness of vertical axis wind turbine for domestic consumers*, 2020 Int. Symp. Adv. Electr. Commun. Technol. ISAECT 2020 (2020).
11. M.S. Genc, K. Sekhoune Ozden, *Flow physics analysis of a vertical axis wind turbine using FloEFD*, 7th Iran Wind Energy Conf. IWEC 2021 (2021).
12. O. Beik, A. Al–Adsani, *Proposed wind turbine limited– and high–speed operation*, 2020 IEEE Electr. Power Energy Conf. EPEC 2020 (2020).
13. H. Tao, *Research on optimization control strategy using model predictive control of wind turbine generators*, 2023 IEEE Sustain. Power Energy Conf. iSPEC 2023 (2023).
14. K. Naoi, M. Shiono, *Relationship between incident angle of wind on rotor blade and output of a drag–type multi-blade vertical–axis wind turbine with stationary multi–vanes*, 2021 11th Int. Conf. Power, Energy Electr. Eng. CPEEE 2021, pp. 147–152 (2021).
15. J. Baruah, P. Venkaiah, N. Kumar, B.K. Sarkar, N. Alom, *Offshore wind turbine pitch control with aeroelastic effect*, 2022 IEEE IAS Glob. Conf. Emerg. Technol. GlobConET 2022, pp. 875–880 (2022).
16. J. Liu, Q. Zhang, R. Zhang, J. Hu, L. Zhang, B. Cai, *An asymmetric–primary axis–flux hybrid–excitation generator for the vertical axis wind turbine*, IEEE Access (2021).
17. M.F. Akorede, *Design and performance analysis of off–grid hybrid renewable energy systems*, Hybrid Technol. Power Gener., pp. 35–68 (2021).
18. ***ABB, *Technical application papers No.13 Wind power plants*, no. 13, p. 136 (2011).
19. A. Biswas, A. Nath, A. Kundu, S. Sarkar, S. Bhowmick, R.S. Pal, *Modelling of wind turbine and study its operation at various input parameters*, 2023 7th Int. Conf. Electron. Mater. Eng. Nano–Technology, IEMENTech 2023 (2023).
20. C.P. Chioncel, O.G. Tirian, M. Dordescu, E. Spunei, *Optimization of wind turbine operation in variable wind speed conditions*, 2020 7th Int. Conf. Energy Effic. Agric. Eng. EE AE 2020 – Proc. (2020).